A prototype of three-dimensional transparent current collector with enhanced charge collection

GUANGWU YANG[a, b,*], FUZHEN ZHAO[a], BING HE[a], WENYUE GUO[a, b], XIAOQING LU[a], QINGZHONG XUE[a, b]

[a]*College of Science, China University of Petroleum, Qingdao, 266580, PR China*
[b]*Key Laboratory of New Energy Physics & Materials Science in Universities of Shandong, China University of Petroleum, Qingdao, 266580, PR China*

We report in this paper a prototype of three-dimensional transparent current collector (3D-TCC) with enhanced charge collection, which is achieved by growing low-density and large diameter ZnO microrod arrays on fluorinated tin oxide (FTO) substrates. Structure, morphology, electrical and optical properties of 3D-TCC are discussed. The charge collection properties of this novel 3D-TCC are studied by comparing it with those of conventional FTO for use as a current collector in dye-sensitized solar cells (DSCs). The electrochemical impedance spectroscopy analysis reveals that the electron transport, electron lifetime, effective diffusion length and the electron collection efficiency are increased, while the charge recombination is reduced, resulting in the remarkably enhanced power conversion efficiency of 7.17%, higher by 17% than conventional DSCs using FTO glass. These results indicate that the proposed 3D-TCC can be considered as a superior electrode for various types of photovoltaic devices.

1. Introduction

The photoelectric conversion efficiency of photovoltaic devices is greatly determined by the charge collection efficiency [1, 2]. To date, most of the photovoltaic devices utilize transparent conducting oxides (TCO) coated on various substrates as the charge collecting electrodes [3-5]. For instance, in dye-sensitized solar cells (DSCs), the commonly used charge collecting electrode is fluorinated tin oxide (FTO) glass or tin-doped indium oxide (ITO) glass [6, 7]. The disadvantage of the TCO layer as a charge collector lies in its planar structure, which means that the photo-generated electrons have to travel long and thus experience millions of trapping events before they are collected (Fig. 1A), which decrease the electron diffusion coefficient and increase the recombination rate [8].

A simple strategy to overcome the disadvantages of two-dimensional current collector (2D-TCC) is to develop it to be a three-dimensional current collector (3D-TCC). A 3D-TCC enables the electrons collected by the nearest current collector from where they are generated, thus shortens the pathway to the back contact and speeds up the transport for the injected electrons (Fig. 1B). This is the basic concept discussed in the article. An example is given on how a 3D-TCC improves the performance of a conventional DSC. First, a prototype of 3D-TCC is constructed by growing low-density and large-diameter ZnO microrod arrays on FTO glass. Second, how this

novel 3D-TCC improve the performance of DSCs is demonstrated by comparing it with that of conventional FTO. Third, Electrochemical Impedance Spectroscopy (EIS) tests are performed to understand why the new 3D architecture is favorable over a 2D geometry.
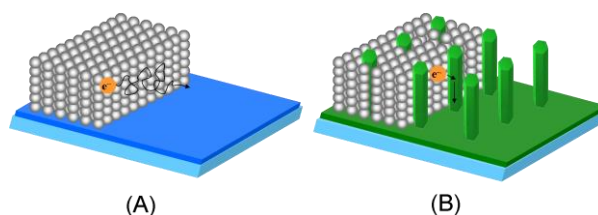
Fig. 1. Schematic illustrations of the photoelectrode structure and the electron transport behaviors of (A) the conventional 2D-TCC, and (B) the proposed 3D-TCC.

2. Experimental

2.1 Preparation of 3D-TCC

For the preparation of 3D-TCC, FTO glasses are cleaned successively by acetone, ethanol, and deionized water sonication. Low-density and large-diameter arrays of ZnO microrods are then grown via a low temperature hydrothermal process at 90 °C for 8 h, which is conducted

by immersing a piece of FTO glass with the conducting side facing down in an aqueous solution containing 0.5 M zinc nitrate ($Zn(NO_3)_2 \cdot 6H_2O$) and 0.5 M hexamethylenetetramine ($C_6H_{12}N_4$).

2.2 Fabrication of porous TiO₂ film on 3D-TCC

Porous TiO_2 film is prepared by screen-printing TiO_2 paste (Dyesol 18NRT) on 3D-TCC several times to get an appropriate thickness. The printed film is then sintered in air by heating gradually to 325 °C and holding for 5 min, then 375 °C for 5 min, at 450 °C for 15 min, and finally at 500 °C for 15 min. No scattering layer and post $TiCl_4$ treatment are employed throughout the study. The thickness of the film is determined by an Alpha-Step IQ surface profiler to be approximately 8 μm.

2.3 DSC assembly

The assembly process of DSCs is similar to that of a conventional DSC reported elsewhere [9]. Typically, the photoelectrode is dyed by soaking in 0.15 mM solution of N719 (Dyesol) in ethanol at room temperature for 12 h. Pt counter electrode is prepared by depositing a thin layer of Pt nanoparticles onto FTO glasses by thermal decomposition of hexachloroplatinic acid. The electrolyte is E008 (MPN based, 0.1 M iodine, 1 M PMII, 0.5 M NMB and 0.1 M LiTFSI). The as-fabricated cells are denoted as 3D-DSC. For comparison, conventional DSCs using FTO glass as a current collector are also assembled under the identical condition, which are denoted as 2D-DSC.

2.4 Characterization

X-ray diffraction (XRD) patterns are collected using a Rigaku D/MAX 2700 diffractometer (Japan) with Cu Kα radiation (k = 1.5418 Å) operating at 40.0 kV, 60.0 mA. The electrical resistivity is measured using the four-probe method. Optical transmittance is studied using a UV–Vis spectrophotometer. Morphology of the 3D-TCC and the 3D-TCC loaded with TiO_2 film are characterized by scanning electron microscopy (SEM, Philips XL 30 FEG). The current-voltage (I–V) characterization are operated using a Keithley Source Meter and the PVIV software package (Newport). Simulated AM 1.5 illumination is provided by a Newport class A solar simulator. EIS measurements are performed using an Autolab potentiostat/galvanostat and the Nova 1.6 software package. The cells are biased to the open-circuit photovoltage in the dark.

3. Results and discussion

3.1. Structure and morphology

Fig. 2A displays the XRD patterns of the reference ZnO powers, FTO glass, and 3D-TCC. All the diffraction peaks located at 2θ values of 20–80° for the ZnO microrods agree well with hexagonal phase ZnO (JCPDS No. 80-0074) without any diffraction peaks. Compared with the powder diffraction patterns, the XRD patterns of ZnO microrod arrays show a dominant diffraction peak corresponding to (002) planes, which indicates that the ZnO microrods are grown with a high orientation of their c-axis perpendicular to the substrate [10]. Fig. 2B show the overview of 3D-TCC. It can be seen that the ZnO microrod arrays are highly uniform over the entire surface of FTO glass, aligning in a quite low density with a mean space of 10 μm and a length of about 10 μm. Inset of Fig. 2B shows the morphology of an individual ZnO rod, with a mean diameter of 1 μm. As expected, the ZnO microrod is oriented approximately perpendicular to the surface of the substrate and possesses a well-defined hexagonal prism morphology. Different from the previous reports on 1D ZnO [11], which are mostly high-density and small-diameter ZnO nanowires/rods, our method produces low-density and large-diameter ZnO microrod arrays, which provide important morphology functions for the 3D-TCC. First, it provides enough interspace for TiO_2 nanoparticle loading, so as to maintain a high surface area for dye adsorption. Second, it facilitates the penetration of TiO_2 paste, which is essential to the formation of a uniform hybrid film and the well contact between ZnO and TiO_2. Third, this strategy involves no sophisticated reactor and vacuum system with mass-production capability [12]. Furthermore, this method requires no pre-prepared ZnO seeds, which is important for the well-developed photovoltaic devices, because for the seed growth method, the seeds would remain in the final ZnO structure, resulting in unfavorable properties. It can be observed that after screen printing (Fig. 2C and D), TiO_2 nanoparticles have been successfully filled into the interspace of 3D-TCC. The resulted TiO_2 film is smooth and compact without any cracks, indicating that the screen printing of TiO_2 paste does not induce any visible structure degradation of 3D-TCC. The ZnO microrods are closely and tightly surrounded by the TiO_2 nanoparticles without any gaps, suggesting a desirable contact between 3D-TCC and TiO_2 nanoparticles.
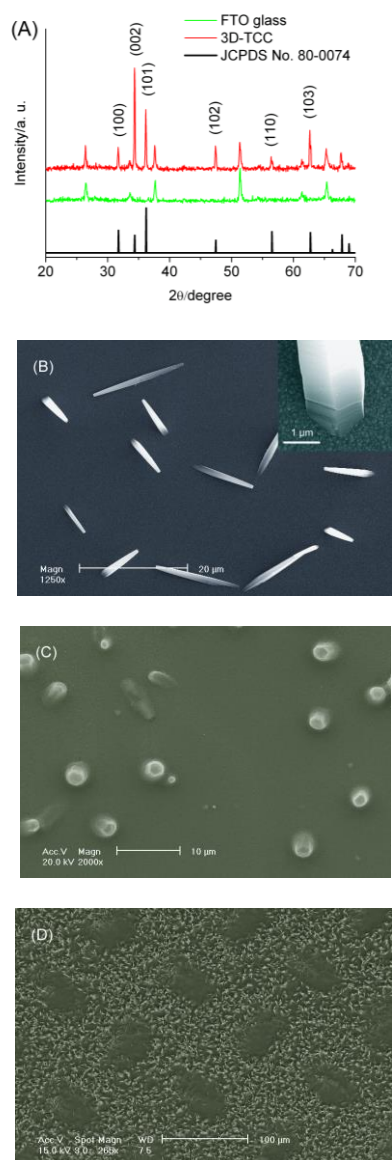
Fig. 2. (A) XRD patterns of the reference ZnO powers, FTO glass, and 3D-TCC; (B) SEM images of 3D-TCC (Inset shows the morphology of an individual ZnO microrod); (C, D) SEM images of 3D-TCC loaded with TiO$_2$ nanoparticles via screen printing technique ((C) at high magnification, and (D) at low magnification)

3.2. Electrical resistivity, transmittance and photocurrent-voltage measurements

The measured sheet resistance of 3D-TCC is 6.8 Ω/□, which is lower than that of FTO glass selected (7.22 Ω/□), indicating its good conductive properties. The transmittance spectra of FTO glass, 3D-TCC, TiO$_2$ film on FTO glass, and TiO$_2$ film on 3D-TCC in the visible and near-infrared band are illustrated in Fig. 3A. The transmission of FTO glass is > 80 % from 400 to 1000 nm, which agrees well with its specifications. Although the transmission of 3D-TCC is lower than that of FTO glass,

which is mainly due to the scattering effect of ZnO microrods, the transmission of > 70 % exhibited by 3D-TCC in the same spectral range demonstrates its qualification as a front electrode for thin film solar cells. The lower transmittance of TiO$_2$ film on 3D-TCC further demonstrates the higher scattering effect of ZnO microrods, because TiO$_2$ merely has negligible absorption in the visible/near-infrared band. In this sense, 3D-TCC may not be the best in its light-harvesting capability. However, compared with 2D-DSC, 3D-DSC shows higher IPCE values over the entire visible light range (Fig. 3B), which mainly attributed to the reduced charge recombination benefitted from ZnO microrods that improve electron transport properties.
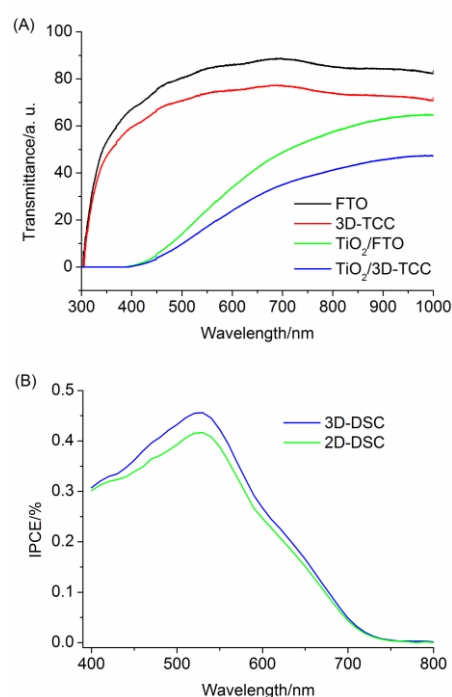
Fig. 3. (A) Transmittance spectra of FTO glass, 3D-TCC, TiO$_2$ film on FTO glass, and TiO$_2$ film on 3D-TCC; (B) IPCE spectra of the 2D-DSC and the 3D-DSC

3.3. Energy conversion characteristics

Fig. 4 shows the comparison of the I–V characteristics for 3D-DSC and 2D-DSC. The V_{OC} and the FF of 3D-DSC tend to decrease, possibly due to the decrease of surface area and roughness factor. The J_{SC} of 3D-DSC is highly increased by ca. 19.5% compared to that of 2D-DSC, which indicates that 3D-TCC would be crucial for obtaining the charge collection enhancement. Based on the increased Jsc, 3D-DSC exhibits a much higher power conversion efficiency of 7.17%, which is increased by about 17% compared with 2D-DSC. It is noticed that no pre- and post TiCl$_4$ treatment and scattering layer are employed through the study, and the film thickness of the

as-fabricated 3D-DSC is adjusted to be 8 μm. Accordingly, the efficiency of the as-fabricated 3D-DSC is lower than that of standard DSCs, which usually possess a typically power conversion efficiency of ca. 10%. The effects of $TiCl_4$ treatment, scattering layer, and film thickness to the cell performance have been well demonstrated [9], and one can get higher efficiency by improving the materials and fabrication procedure based on our designing. These results demonstrate application of this 3D-TCC as a replacement for 2D FTO TCC.
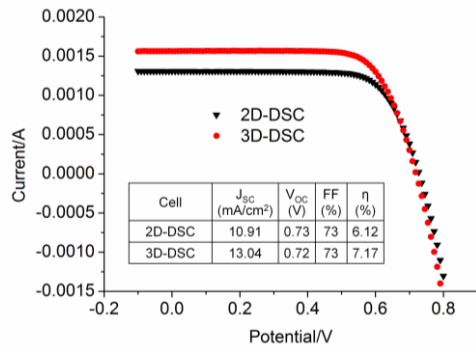
Fig. 4. I–V characteristics curves of the 2D-DSC and the 3D-DSC. Inset shows the summarized results of the open circuit voltage (V_{oc}), short-circuit current density (J_{sc}), fill factor (FF), and power conversion efficiency (η)

3.4. Electrochemical impedance measurements

EIS provides the information of capacitance and resistance of the electrode materials, which is an effective approach for investigating electron transport and recombination properties across the electrolyte and the surface of the electrode. Fig. 5 illustrates the typical impedance spectra (Nyquist plots) for 3D-DSC and 2D-DSC. The derived parameters are presented in Table 1 after the data being fitted by a proper equivalent circuit [13]. The decrease of R_t and the increase of R_{ct} reveal that 3D-TCC serves here not only as transport paths but also as trapping sites to prevent electrons recombining with the electrolyte, which is further verified by the increase of C_μ. Because the value of C_μ gives the total density of free electrons in the conduction band and the localized electrons in the trapping sites [14]. The longer lifetime implies a lower recombination rate and an enhanced charge collection efficiency. Furthermore, the higher values of electron diffusion length and electron collecting efficiency exhibited by 3D-DSC demonstrate the enhancement of charge collection efficiency.
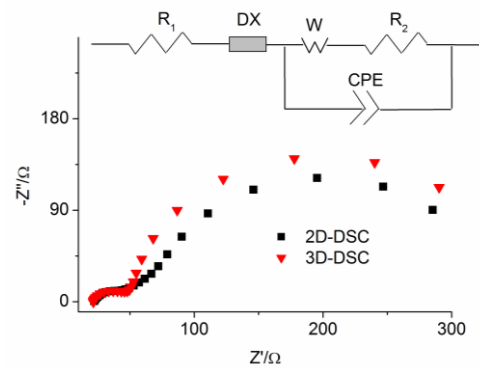
Fig. 5. Nyquist plots of the 2D-DSC and the 3D-DSC. Inset is the fitted equivalent circuit for impedance analysis

Table 1. Electron properties of the cells

Cell	R_t (Ω)	R_{ct} (Ω)	C_μ (μF)	τ_n (ms)	L_n (μm)	η_{ec}
2D-DSC	28.74	141.3	471.3	66.6	22.2	79.7
3D-DSC	19.37	223.2	771.6	172.2	33.9	91.3

R_t: impedance of electron transport in photoelectrode; R_{ct}: impedance of electron recombination with the electrolyte; C_μ: chemical capacitance; τ_n: electron lifetime; L_n: effective diffusion length; η_{ec}: electron collecting efficiency

4. Conclusions

In summary, we have proposed for the first time a prototype of 3D-TCC and demonstrated its application for enhancing the charge collection in photovoltaic devices. DSCs employing 3D-TCC as a current collector exhibit an encouraging power conversion efficiency of 7.17%, higher by 17% than conventional DSCs using 2D FTO glass, owing to the facilitated electron transport and retarded charge recombination. This work provides a basis for further development in improving the photovoltaic device efficiency via the application of 3D-TCC.

References

[1] W. U. Huynh, J. J. Dittmer, A. P. Alivisatos, Science **295**, 2425 (2002).
[2] B. Tian, T. J. Kemap, C. M. Lieber, Chem. Soc. Rev. **38**, 16 (2009).
[3] M. Grätzel, Photoelectrochemical cells, Nature **414**,

338 (2001).

[4] C. J. Brabec, S. Gowrisanker, J. J. M. Halls, D. Laird, S. Jia, S. P. Williams, Adv. Mater. **22**, 3839 (2010).

[5] J. Tang, E. H. Sargent, Adv. Mater. **23**, 12 (2011).

[6] B. X. Lei, J. Y. Liao, R. Zhang, J. Wang, C. Y. Su, D. B. Kuang, J. Phys. Chem. C **114**, 15228 (2010).

[7] O. Lupan, V. M. Guerin, I. M. Tiginyanu, V. V. Ursaki, L. Chow, H. Heinrich, T. Pauporte, J. Photochem. Photobio. A **211**, 65 (2010).

[8] S. Gubbala, V. Chakrapani, V. Kumar, M. K. Sunkara, Adv. Funct. Mater. **18**, 2411 (2008).

[9] S. Ito, T. N. Murakami, P. Comte, P. Liska, C. Grätzel, M. K. Nazeeruddin, M. Grätzel, Thin Solid Films **516**, 4613 (2008).

[10] S. Pang, T. F. Xie, Y. Zhang, X. Wei, M. Yang, D. J. Wang, J. Phys. Chem. C **111**, 18417 (2007).

[11] M. Law, L. E. Greene, J. C. Johnson, R. Saykally, P. D. Yang, Nat. Mater. **4**, 455 (2005).

[12] N. Tetreault, E. Arsenault, L. P. Heiniger, N. Soheilnia, J. Brillet, T. Moehl, S. Zakeeruddin, G. A. Ozin, M. Gratzel, Nano Lett. **11**, 4579 (2011).

[13] R. Kern, R. Sastrawan, J. Ferber, R. Stangl, J. Luther, Electrochim. Acta **47**, 4213 (2002).

[14] Q. Wang, S. Ito, M. Grätzel, F. Fabregat-Santiago, I. Mora-Sero, J. Bisquert, T. Bessho, H. Imai, J. Phys. Chem. B **110**, 25210 (2006).

_____

*Corresponding author: yanggw@upc.edu.cn